Aerospace **2015**, *2*, 482-504; doi:10.3390/aerospace2030482

OPEN ACCESS

aerospace

ISSN 2226-4310

www.mdpi.com/journal/aerospace

Article

Decamber Morphing Concepts by Using a Hybrid Trailing Edge Control Surface

Yavuz Yaman *, İlhan Ozan Tunçöz †, Yosheph Yang †, Pınar Arslan †, Uğur Kalkan †, Harun Tıraş †, Ercan Gürses †, Melin Şahin † and Serkan Özgen †

Department of Aerospace Engineering, Middle East Technical University, METU, Ankara 06800, Turkey; E-Mails: ozan.tuncoz@metu.edu.tr (İ.O.T.); yosheph.yang@metu.edu.tr (Y.Y.); pinar.arslan@metu.edu.tr (P.A.); ugur.kalkan@metu.edu.tr (U.K.); tiras.harun@metu.edu.tr (H.T.); gurses@metu.edu.tr (E.G.); msahin@metu.edu.tr (M.Ş.); serkan.ozgen@ae.metu.edu.tr (S.Ö.)

† These authors contributed equally to this work.

* Author to whom correspondence should be addressed; E-Mail: yyaman@metu.edu.tr;
Tel.: +90-312-210-4285; Fax: +90-312-210-4250.

Academic Editor: Rafic Ajaj

Received: 21 May 2015 / Accepted: 14 July 2015 / Published: 28 July 2015

Abstract: The idea of morphing is drawing extensive attention in aerospace technologies. Several different approaches like span, camber, twist, and sweep are finding applications. In this work, the concept of a trailing edge control surface which is capable of performing decamber morphing is explained. The upper and lower parts of the control surface undergo different chordwise elongations and the difference between these displacements gives rise to either camber or decamber morphing. The necessary force is achieved by the help of servo actuators. During the design, the structural analyses were done to determine the best viable options for the number of servo actuators, the location of the servo actuators, and the material properties used in the control surface. The control surface was designed of aluminum, composite and compliant materials hence was called a hybrid one. The structural analyses were conducted by using ANSYS® Workbench v14.0 package program. After finding the best viable design, which was made for *in vacuo* condition, the proposed design was also verified under the simulated aerodynamic loading. The aerodynamic loads were obtained from CFD analyses which were done with SU2 V3.2.3 open-source flow solver.

Keywords: camber morphing; hybrid control surface; structural analysis; finite element method

---

1. Introduction

The presence of morphing technology in the aircraft design has allowed the aircraft to change its shape. The shape variation that an aircraft can produce helps the aircraft to attain a better performance and efficiency in a wider range of flight mission [1]. In other words, the morphing aircraft has the capability to perform an optimized aerodynamic performance in other flight missions rather than a specific flight mission. As a result, many researchers have attempted to develop some morphing techniques in order to get a better aircraft performance and efficiency.

The idea of shape changing in the wings of an aircraft was started by the Wright Brothers. At that time, they developed a camber and twist variation on the wing shape [2]. In the recent decades, many new concepts of morphing have been applied as well. In their work, Barbarino *et al.* [3] have made a chronological summary about the application of morphing concept on the fixed wing started from 1903 to 2010.

These morphing concepts can be classified into three different criteria in terms of shape variation: planform morphing (includes the variation span, sweep, and chord of the wing), out-of-plane morphing (includes the variation in twist, dihedral, and span-wise bending), and airfoil adjustment morphing (concerns of thickness and camber of the airfoil section) [3].

The morphing technology has some major drawbacks in the application. One major drawback is that a morphing wing often requires complex mechanisms which increase the installation and maintenance costs [4]. Another major issue is the additional weight that the complex mechanisms bring. Furthermore, the structural analysis and design of morphing wings are also more complicated due to these issues. Consequently, conventional sizing approach also becomes insufficient and requires far more complicated methods.

Regarding the design of a camber variable wing, Shilli *et al.* [5] categorized three different methods to perform it: the conventional hinged mechanism, the smart-material-made actuators, and the compliant mechanism. Despite the easy integration and simple actuation that conventional control surface has, this system also have some major drawbacks. The existing discontinuities produced by the conventional control surfaces may result in flow separation and increase in drag [3]. Conversely, the unconventional control surfaces with the smart-material-made actuators and the compliant mechanisms can provide smooth shape changes along the wing surface, hence, can decrease the adverse effects of the conventional ones.

There have been many research studies concerning adaptive trailing edge control surfaces. Smart Wing Program, which was funded by Defense Advanced Research Program Agency (DARPA) is one of them. A trailing edge control surface composed of elastomeric (silicone) outer skin, flexible honeycomb and fiberglass laminate as a center leaf is one of the concepts developed under this program. While the honeycomb part is responsible for increasing the resistance to vertical loads, the silicone skin which undergoes large deformations provides a smooth shape change and reduces the actuation forces in this concept. Additionally, the chordwise shape of the control surface is stabilized by the laminate part [6].

Within the context of morphing trailing edge development, the German Aerospace Center (DLR) investigates two different concepts for the camber variation. The first concept is the finger concept trailing edge design, having a metallic flexible skin whose aim is to achieve a smooth aerodynamic profile. The ribs of the concept are modelled by combining separate plate-like elements (fingers) with revolute joints [7]. A transmission beam, which groups the ribs, is designed in order to reduce the number of actuators to be utilized. Consequently, the trailing edge control surface with finger concept deforms into an arc-like shape [8]. The second design of the DLR is the belt rib control surface concept where the skin is modelled like a belt and the ribs are designed like spokes. The desired camber variation shape change of the trailing edge control surface is achieved by altering the angle of the spokes, which connect the upper and lower parts of the belt [9]. More information about the morphing control surfaces can be found in the author's thesis work [10].

In this paper, the idea of a novel camber morphing mechanism is introduced for the trailing edge of an unmanned aerial vehicle wing. In the developed concept the gap, which exists between the wing and the control surface in conventional designs, is eliminated, thereby a smooth flow over the wing-box and the trailing edge is provided. This hybrid trailing edge control surface was developed within the scope of CHANGE (Combined morphing assessment software using flight envelope data and mission based morphing prototype wing development) Project financed under the 7th Framework Program of the European Commission [11].

The baseline unmanned aerial vehicle wing has a NACA 6510 cross section with half span equals to 2 m and no pre-twist along the wing span. The control surface started 10 cm from the root of the baseline wing. Figure 1 depicts the geometry of the half span wing and the location of the control surface.

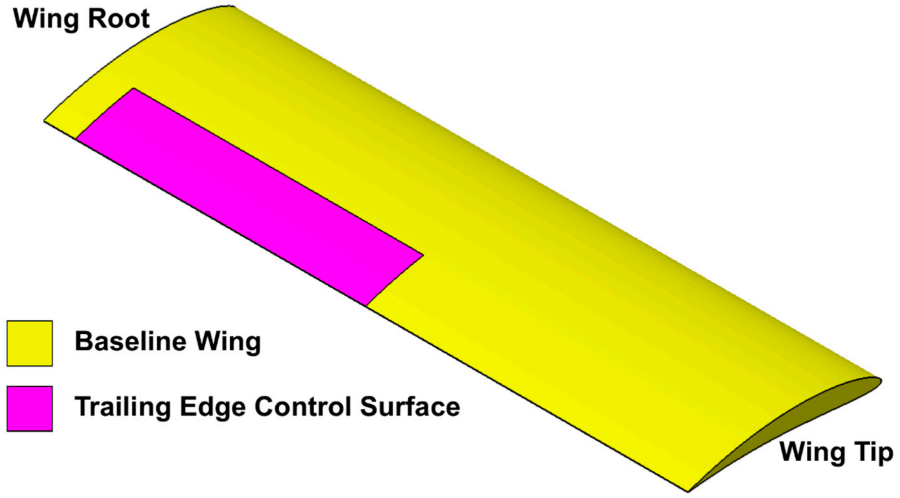

Figure 1. Baseline wing geometry.

The main purpose of the structural design was to achieve a minimum torque for the required morphing value. Hence, several structural design configurations have been tried. The differences between the configurations comprise the properties of the material used in the design, and the number and location of the servo actuators used in the design.

This paper first gives the structural design followed by the details of the Finite Element Analysis (FEA) used in the design process. The comparative studies were conducted *in vacuo* in order to get an optimum design is then elaborated. Computational Fluid Dynamics (CFD) analysis done in order to get the aerodynamic loads is followed by the analyses of the control surface under the simulated aerodynamic loading.

2. Structural Design

The structural design of the morphing trailing edge concept is explained in this section. It is mainly focused on the description of the design; the materials, the number and location of the servo actuators used in the design. The effects of variation of these variables on the design are considered during the design trade-off studies.

In the study two different design concepts were undertaken. The difference was based on the section called the "transmission part" which is the part used to transfer the forces from the servo actuators to the control surface. When there are two separate transmission parts the concept is called the open cell design and when there exists only a single transmission part it is called the closed cell design. Both of the proposed designs have three common components as the C-Part, the compliant part and the composite part. The details of both open cell and closed cell designs are shown in Figures 2 and 3, respectively.

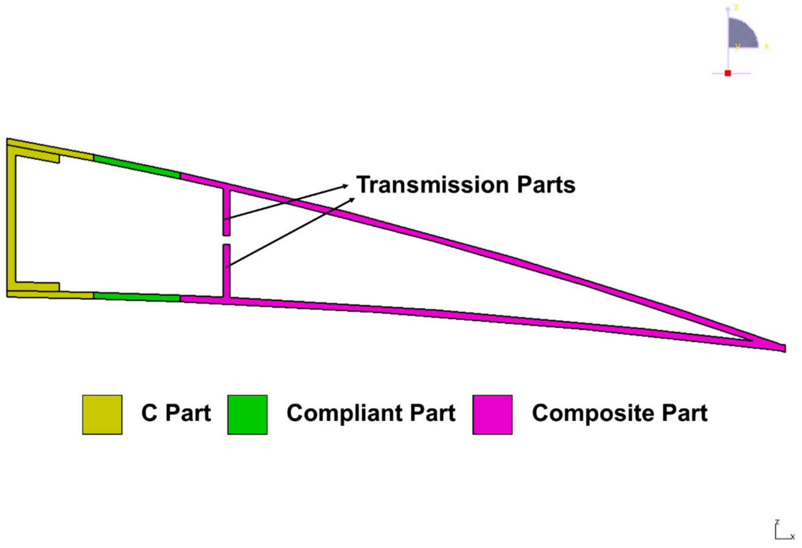

Figure 2. Hybrid trailing edge open cell control surface design.

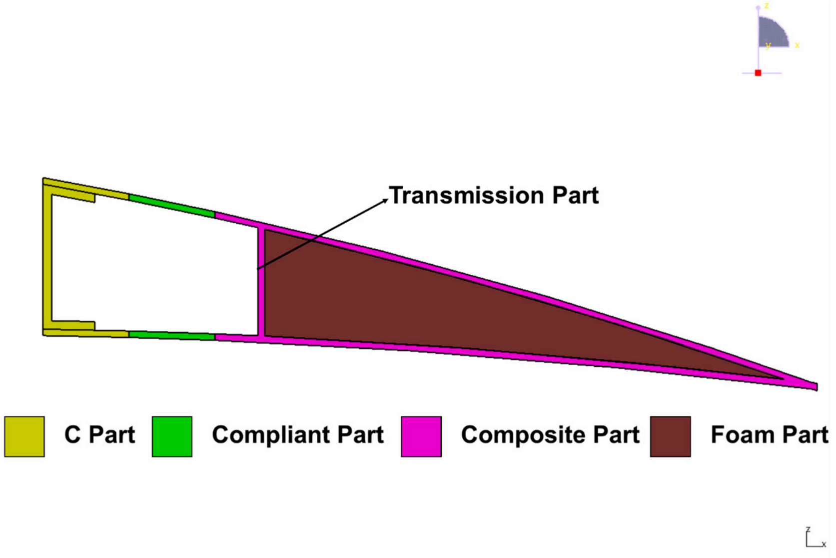

Figure 3. Hybrid trailing edge closed cell control surface design.

During the closed-cell design a foam material is placed inside the available volume in the composite part in order to increase the transverse stiffness of the control surface under aerodynamic loads. The presence of the foam material inside the control surface itself is illustrated in Figure 3. The Rohacell® 51 RIMA [12] was used as the foam material and the properties of this material is given in Table 1.

Table 1. Material properties of Rohacell® 51 RIMA foam [12].

Properties	**Values**
Density, ρ	52 kg/m^3
Young's Modulus, *E*	75 MPa
Shear Modulus, *G*	24 MPa

The C-Part component was used as the connection part, which connects the control surface to the wing. The material used for C-Part is aluminum and Table 2 provides information concerning the material properties.

Table 2. Material properties of the aluminum used in the C-Part [13].

Properties	**Values**
Density, ρ	2770 kg/m^3
Young's Modulus, *E*	71 GPa
Poisson's Ratio, ν	0.33
Tensile Yield Strength	280 MPa
Tensile Ultimate Strength	310 MPa

The compliant part was made by a very flexible material in such a way that it can undergo a significant amount of deformation. The main principle implemented in the control surface is to have tension in both upper and lower compliant parts during the actuation. This is necessary in order to avoid any possible slack in the compliant part which could easily occur in the case where the compliant part was subjected to compression. Then, the difference in the elongations of both compliant parts will give rise to required decamber behavior.

During the study two different materials were proposed for the compliant part: neoprene rubber and a silicone-based material. The density of neoprene rubber is used as 1250 kg/m^3 [14].

Another material used for the compliant part is a silicone based material provided by INVENT GmbH [15]. A uniaxial tension test was conducted in Middle East Technical University, Department of Aerospace Engineering, in order to obtain the stress-strain curve of the material. The density of the silicone-based material was taken as 1250 kg/m^3 [14]. The uniaxial stress-strain curves of neoprene rubber and the silicone are shown in Figure 4.

The composite part is made of glass-fiber prepreg EHG250-68-37 [15], which is significantly stiffer as compared to the compliant part of the control surface. Due to this fact when there are in plane deflections in the upper and lower compliant parts the composite part deflects as if it is undergoing a rigid body rotation. The properties of the composite used in the rigid part are given in Table 3.

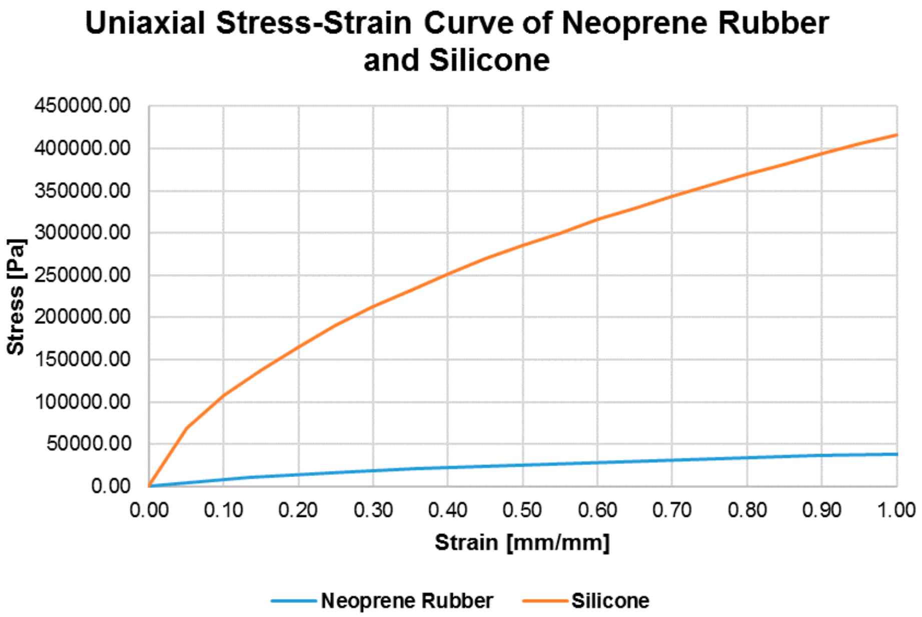

Figure 4. The uniaxial stress-strain curves of neoprene rubber [13] and silicone.

Table 3. Material properties of glass-fiber prepreg EHG250-68-37 composite [14].

Properties	**Values**
Density, ρ	1900 kg/m^3
Young's Modulus, E_{11}	24.5 GPa
Young's Modulus, E_{22}	23.8 GPa
Poisson's Ratio, ν_{12}	0.11
Shear Modulus, G_{12}	4.7 GPa
Shear Modulus, G_{13}	3.6 GPa
Shear Modulus, G_{23}	2.6 GPa
Ply Thickness	0.25 mm

The Servo Actuators

The main actuation mechanism used in the developed morphing concept was the servo actuator. There were two approaches analyzed in this study. In the first one, two servo actuators were used to actuate the upper part of the control surface and another two servo actuators were utilized in order to actuate the lower part of the control surface. In the second one, a total of five servo actuators were utilized. In that configuration two servo actuators actuate the upper part of the control surface and three servo actuators utilized for the actuation of the lower part of the control surface. Hence, both the numbers and the locations of the servo actuators were studied and their effects on the design were evaluated.

Since the servo actuators were placed within the trailing edge control surface, very small sized servo actuators were used in the design due to the very restricted available space. Considering the available torque that servos can provide; it has been determined that Volz DA 13-05-60 servo actuator whose can meet the requirements. The CAD model of the servo actuator is shown in Figure 5 and specifications are given in Table 4.

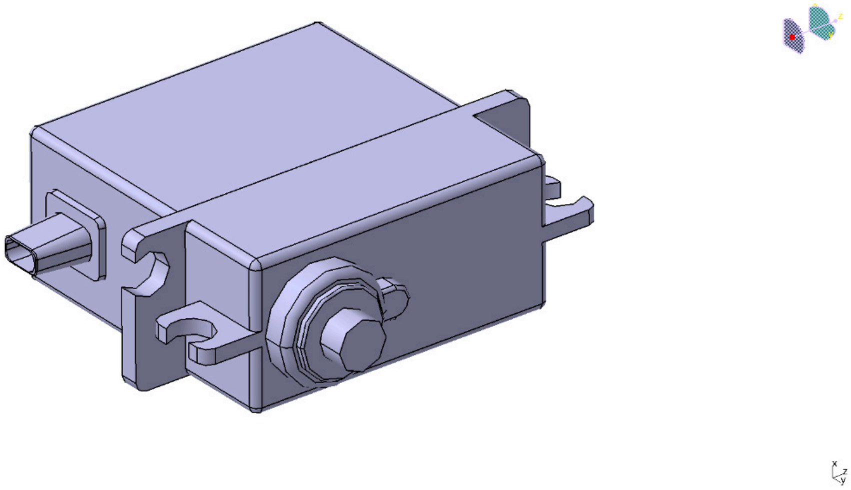

Figure 5. CAD model of Volz DA 13-05-60 servo actuator [16].

Table 4. The specifications of Volz DA 13-05-60 servo actuator [16].

Parameters	**Values**
Operating Voltage	5 V
Peak-Torque	600 N-mm
Weight	19 g
Dimensions	28.5 mm × 28.5 mm × 13 mm

Figures 6 and 7 illustrate the top and isometric view of the configuration for four servo actuators, respectively. On the other hand, Figures 8 and 9 show the top view and isometric view of the configuration for five servo actuators, respectively.

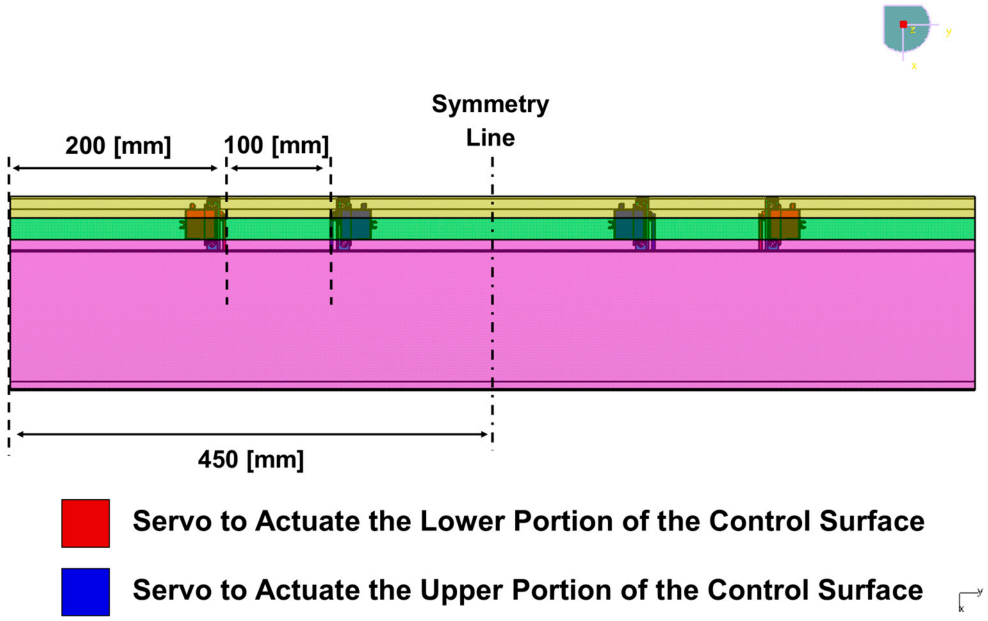

Figure 6. Top view of servo actuators in a four servo actuator configuration.

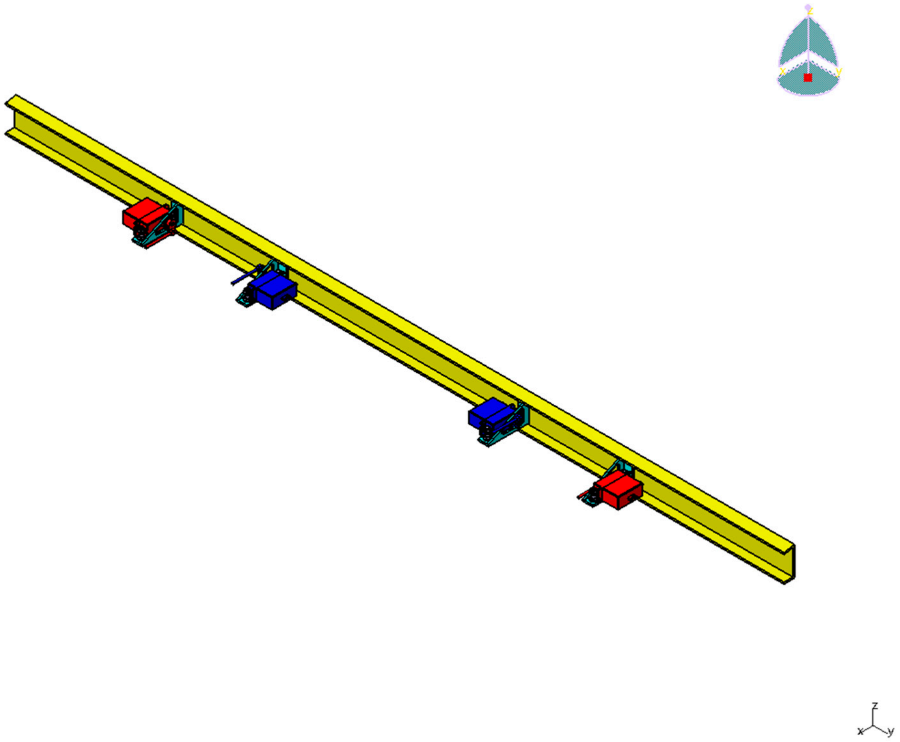

Figure 7. Isometric view of servo actuators in a four servo actuator configuration.

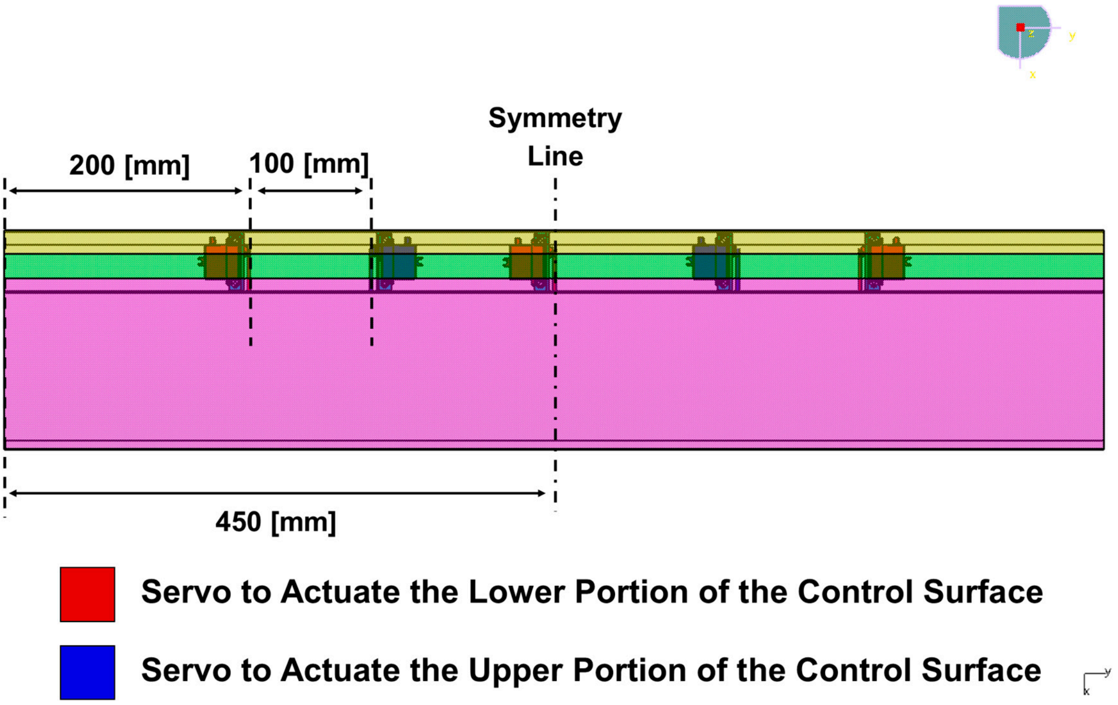

Figure 8. Top view of servo actuators in a five servo actuator configuration.

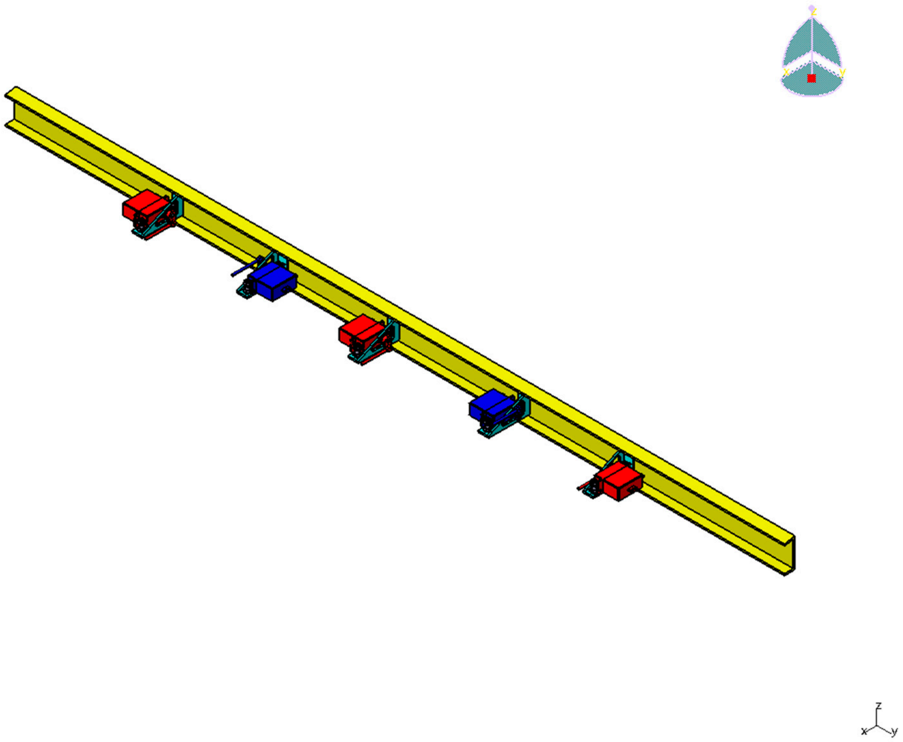

Figure 9. Isometric view of servo actuators in a five servo actuator configuration.

3. Finite Element Analysis

The designed control surface was then analyzed by using Finite Element Method in ANSYS Workbench v14.0 [13]. In this section, finite element modelling for both open cell and closed cell are explained. The generated geometries used for the Finite Element Modeling of open cell design and closed cell design are shown in Figures 10 and 11, respectively.

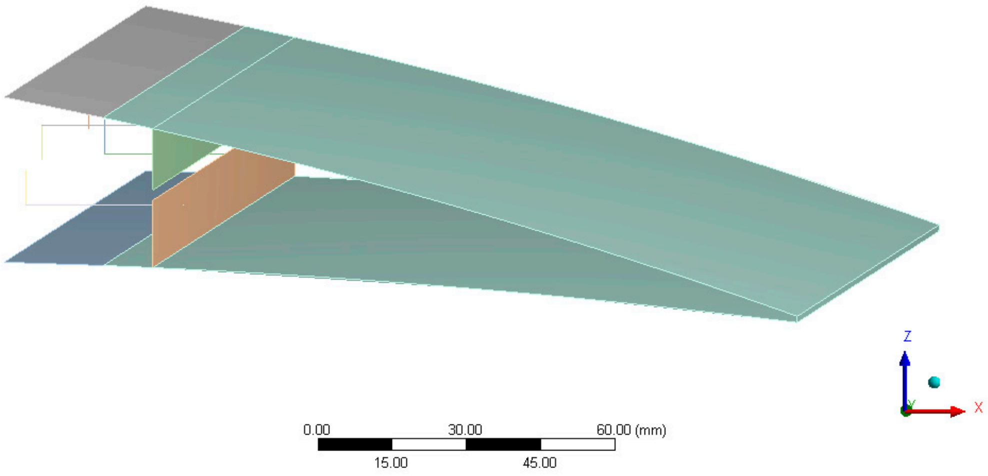

Figure 10. The geometric model of open cell design for finite element model.

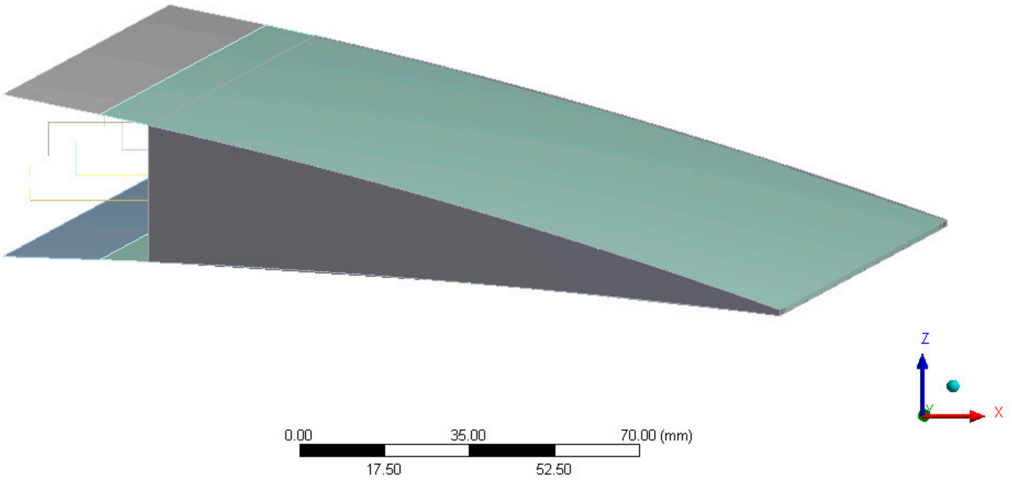

Figure 11. The geometric model of closed cell design for finite element model.

3.1. Meshing Strategy

In the finite element analysis, in order to get a reliable analysis a mesh convergence study is generally conducted before determining the best viable mesh sizing to be used. This sizing is applied for both compliant and composite parts of the control surface. In the current analysis the relevant mesh convergence study was conducted by considering the maximum transverse tip deflection of the control surface as the objective function. Figure 12 summarizes the results of the convergence analyses based on changing quadrilateral element sizes. It can be seen that as the mesh size decreases from 15 (mm) and mesh is getting dense, it converges for 7.5 and 10 (mm) mesh sizes. Further reduction in element sizes was found to yield diverging results because of the fact that the shell theory used for the elements was no longer applicable with specified smaller element sizes.

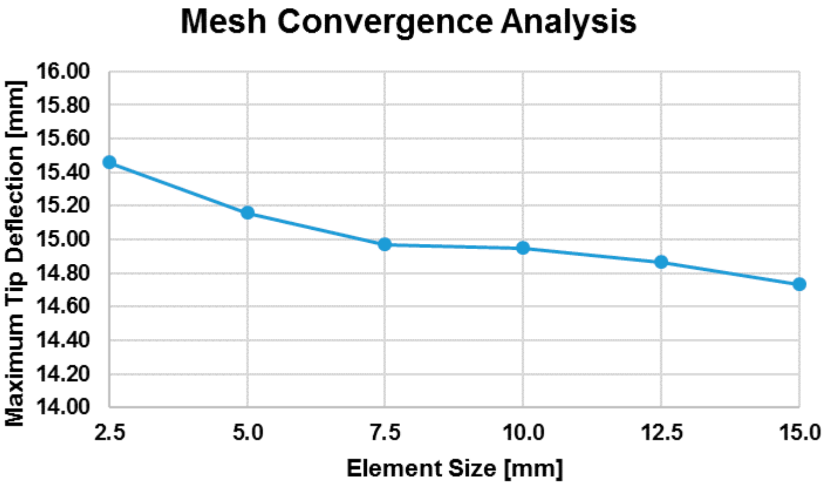

Figure 12. Mesh convergence analysis for finite element analysis.

Several element types were implemented in the finite element model. The details of the element types used in the study are shown in Table 5. Figures 13 and 14 give the generated mesh used in the finite element analysis for open cell design case. Conversely, similar information for the closed cell design are provided in Figures 15 and 16.

Table 5. Meshing used in the finite element modelling.

No.	Model Type	Implemented Geometry	Element Type	Element Size/Cross-Section (for Beam Elements)
1	Surface Body	Composite Part	4-Noded 1st Order Quadrilateral Shell Element	10 mm
		Compliant Part		10 mm
2	Line Body	Moment Arms	2-Noded 1st Order Beam Element	Rectangle: 7.4 mm × 1.9 mm
		Actuation Rods		Circle: radius = 1.25 mm
3	Solid Body	Foam Material	8-Noded 1st Order Solid Element	10 mm

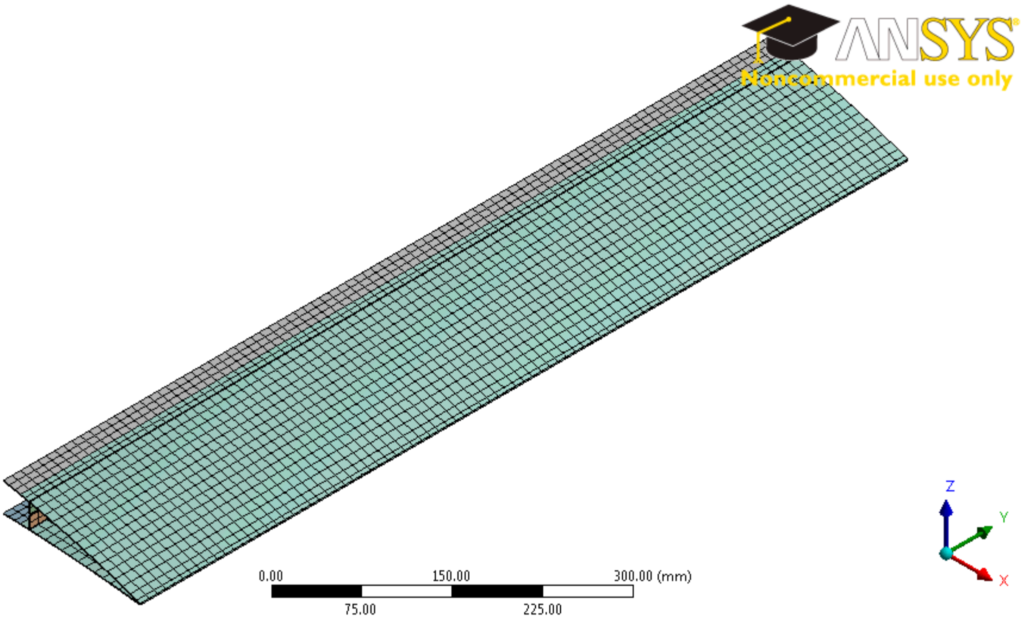

Figure 13. Isometric view of generated mesh for open cell design.

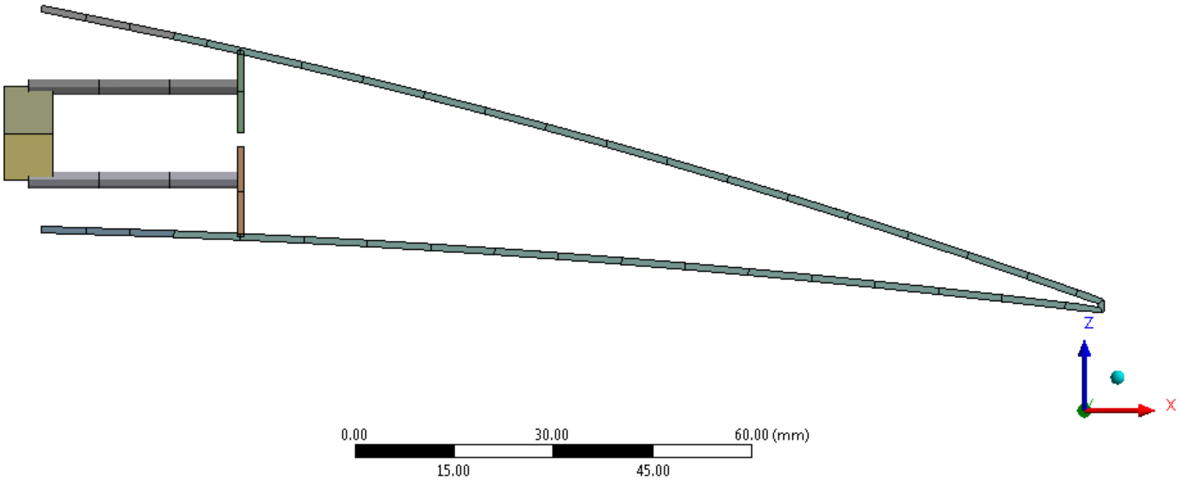

Figure 14. Side view of the generated mesh for open cell design.

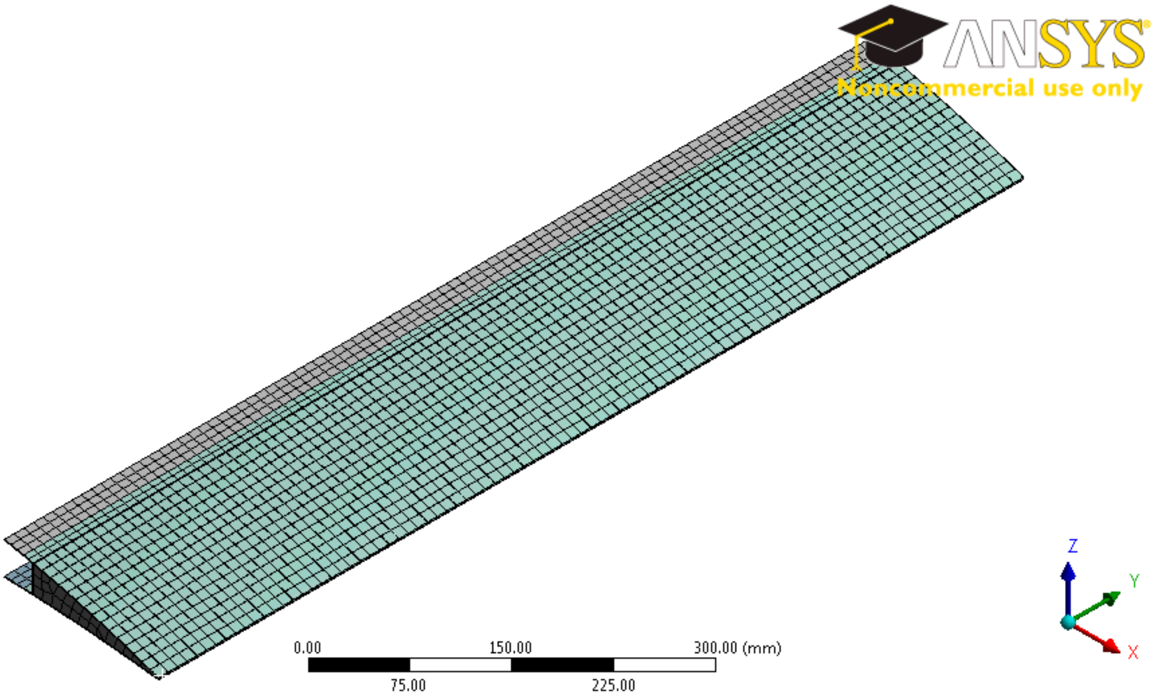

Figure 15. Isometric view of generated mesh for closed cell design.

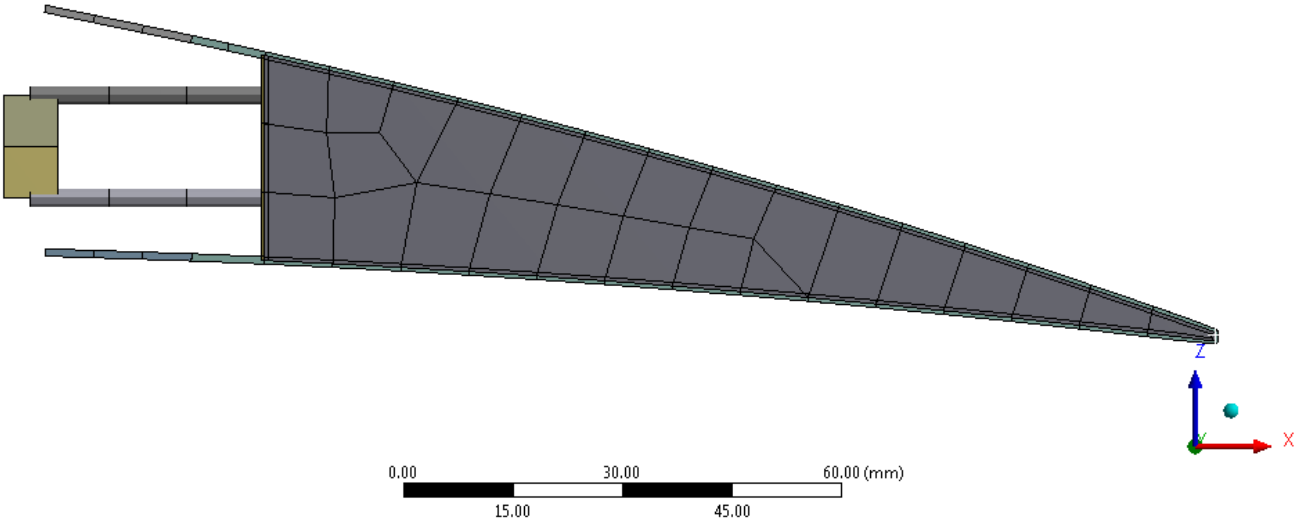

Figure 16. Side view of generated mesh for closed cell design.

3.2. Finite Element Modelling

In order to connect actuation rods to the transmission parts, the bonded contact property of ANSYS was used. By doing so, the model enables servo actuators to transmit their forces to the control system via transmission parts. Figure 17 depicts the region where this type of boundary condition is applied.

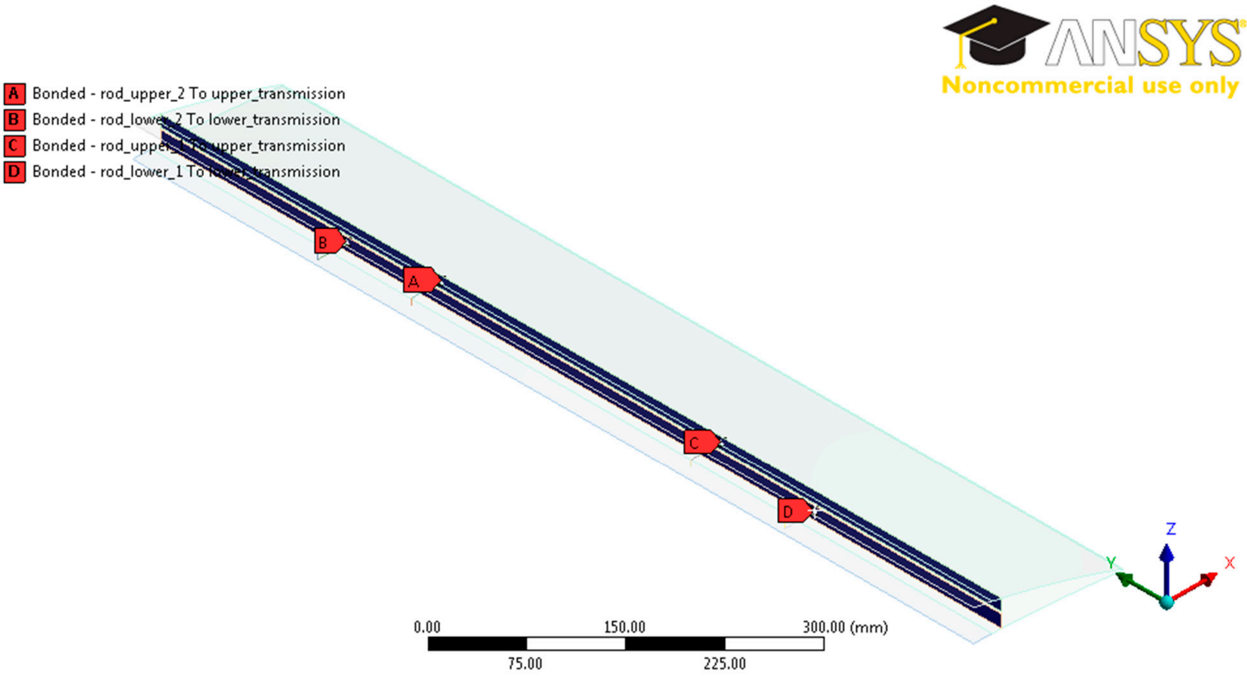

Figure 17. Coinciding edges of compliant part, rigid part, and skin parts of C part.

The servo actuator moment arm and the actuation rod were connected by using the pin-joint mechanism. This pin-joint was modelled by coupling all displacements and rotations, except for rotation about *y* axis, at the coinciding nodes of the actuator moment arms and actuation rods. Figure 18 depicts the so-treated coinciding nodes, representing one case for the lower part actuating servo actuator and one for the upper part actuating servo actuator.

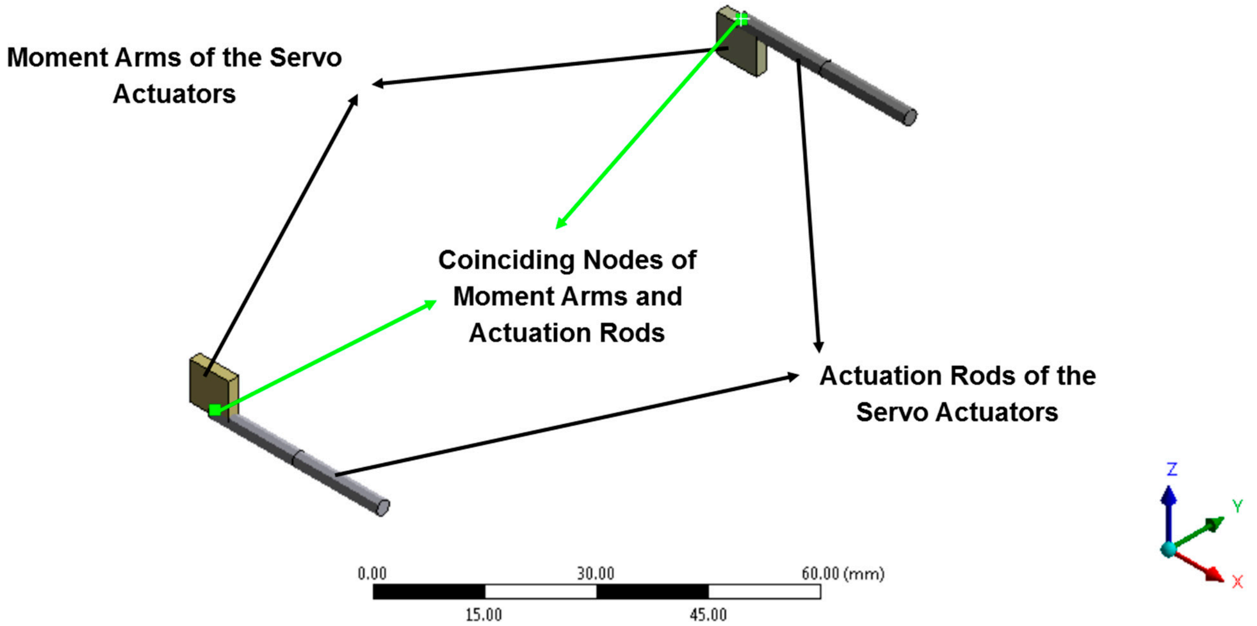

Figure 18. The sample coinciding nodes of servo actuator moment arms and actuation rods.

3.3. Boundary Conditions

During the finite element analyses, the following boundary conditions were used. Both lower and upper edges of the compliant part were specified as fixed supports. The required rotations given as rotational boundary condition was prescribed at the moment arm of the servo motor. Depending on the designed configuration, the given rotations were different. In order to include the weight of the control surface, standard Earth gravity was also applied to the model.

4. Parametric Studies

Explanations about Design Configurations

In this section, five different design configurations are studied and compared. The configurations, with their specific features, are given in Table 6. All of these configurations have NACA 6510 as the initial shape of trailing edge control surface. The structural analyses were conducted in order to morph the control surface into NACA 2510 profile, which is expected to be the maximum decamber capability of control surface. While achieving that, the primary concern was the torque requirement of the servo actuators. The minimum number of servo actuators which satisfy the torque requirements was selected. During the analyses the effects of different compliant materials, different composite cell design and different material thicknesses were also highlighted. The early design studies of the project provided the spanwise actuator locations. Hence those locations were used without further reference.

Table 6. Configurations and respective characteristics of different designs.

Configuration Number	Features
1	Open cell, Neoprene rubber, 4 servo actuators (2 servo actuator push lower side, 2 actuators push upper side). Skin thickness 1 mm.
2	Open cell, Silicone material, 4 servo actuators (2 servo actuator push lower side, 2 actuators push upper side). Skin thickness 1 mm.
3	Closed cell, Silicone material, 4 servo actuators (2 servo actuator push lower side, 2 actuators push upper side). Skin thickness 1 mm.
4	Closed cell, Silicone material, 5 servo actuators (3 servo actuator push lower side, 2 actuators push upper side). Skin thickness 1 mm.
5	Closed cell, Silicone material, 5 servo actuators (3 servo actuator push lower side, 2 actuators push upper side). Skin thickness 0.75 mm.

All the above configurations are first checked under *in vacuo* conditions. The best viable configuration was chosen from these five proposed configurations by considering the criteria of minimum torque values in order to perform the intended morphing to NACA 2510. Figures 20–24 depict the deformation contour for all the design configurations. In Figures 21–25, the servo actuator actuation rods, highlighted in Figure 19, attached to the composite part and push that part. By the comparison of the figures, it can be seen that the maximum transverse displacement can be achieved by the application of Configuration 5.

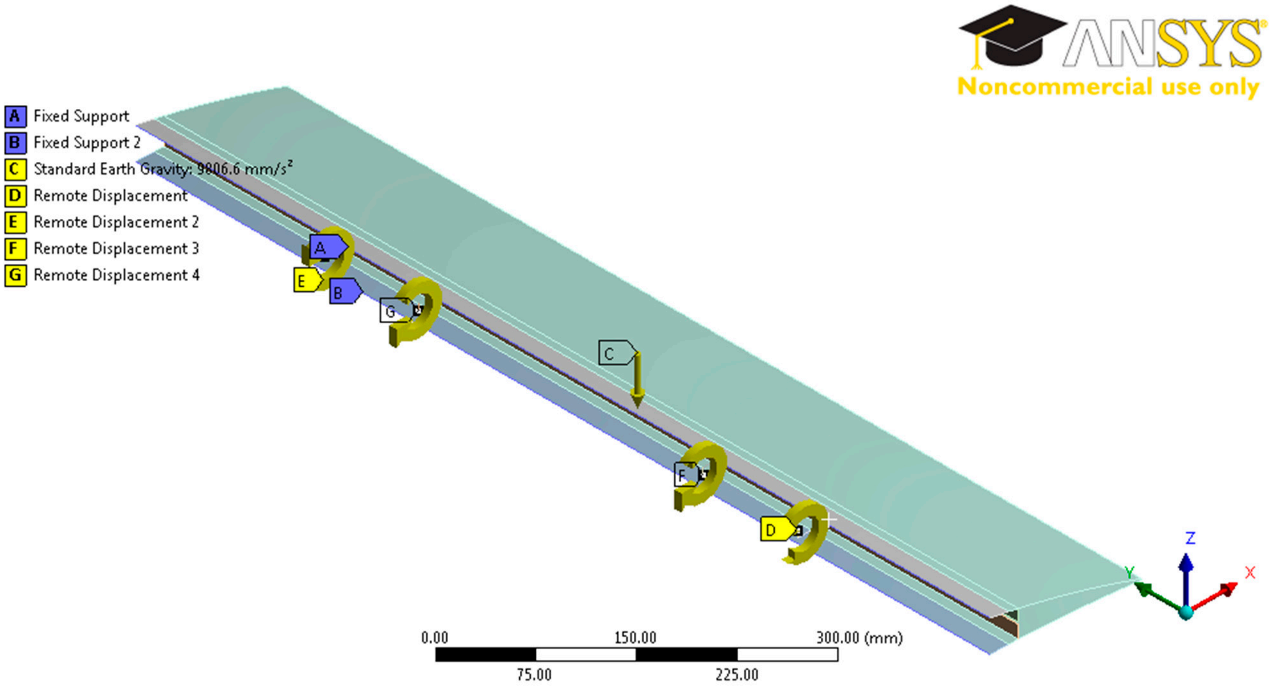

Figure 19. Boundary Condition applied to the leading edge of the rigid part.

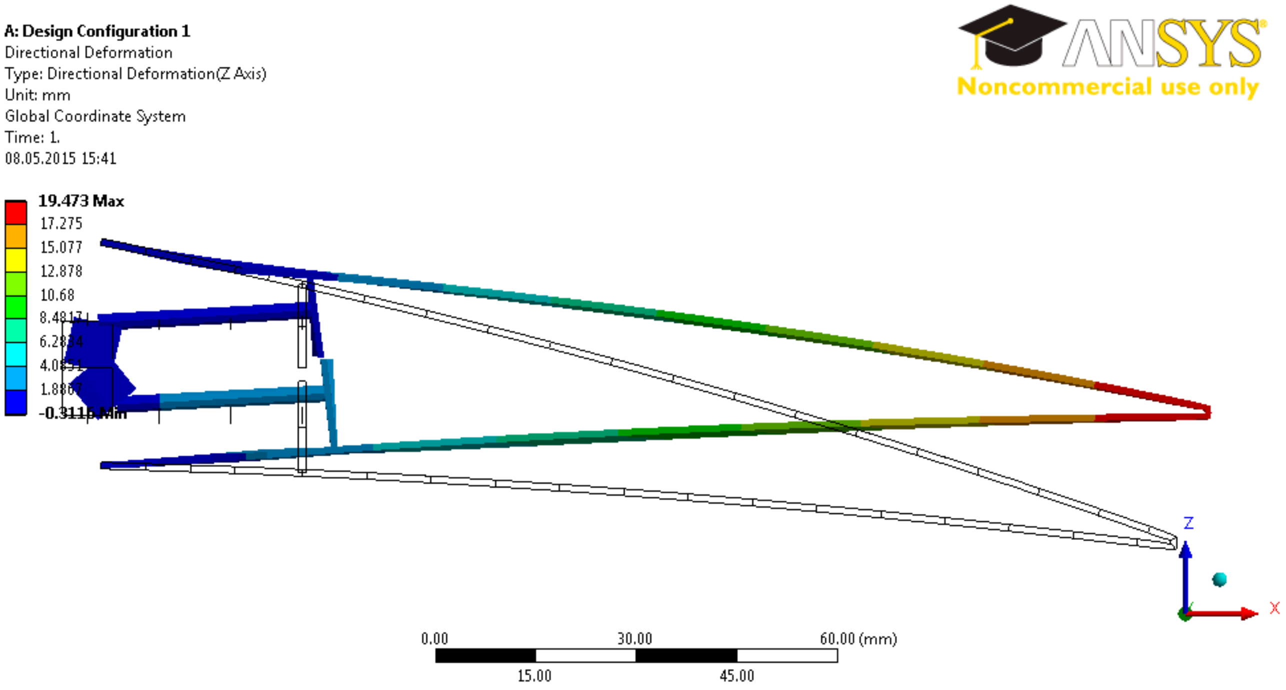

Figure 20. Deformation along *Z*-axis for design configuration 1.

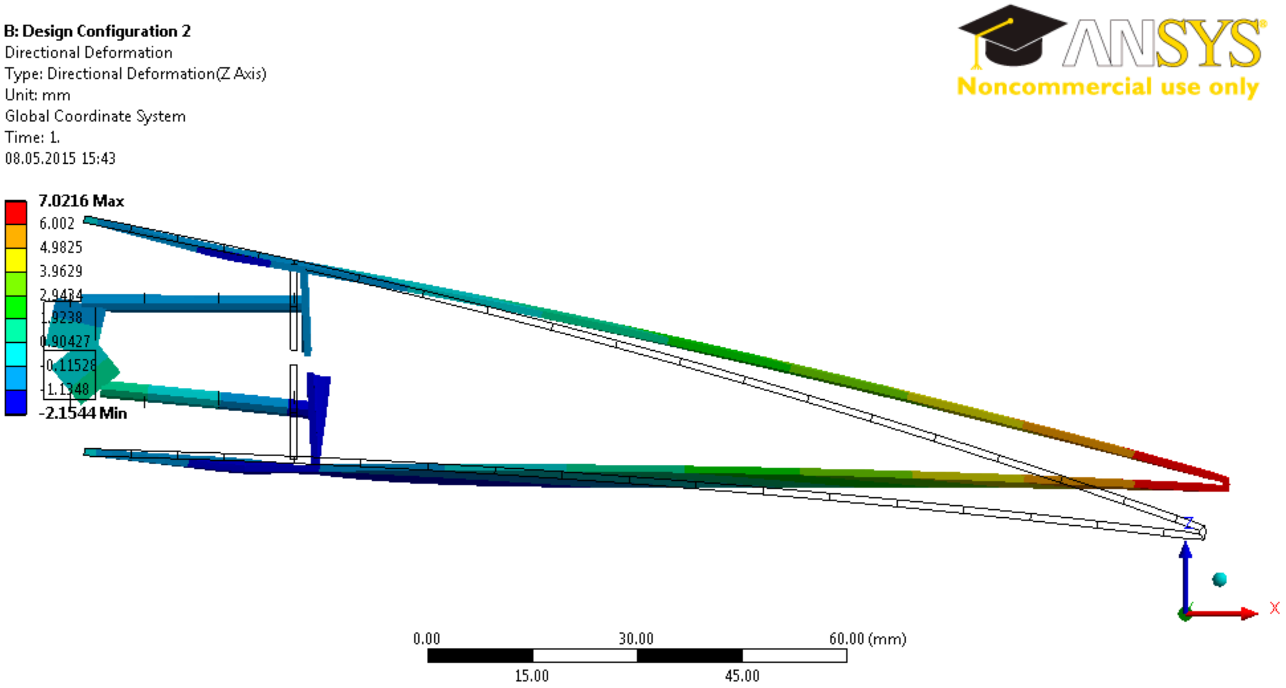

Figure 21. Deformation along *Z*-axis for design configuration 2.

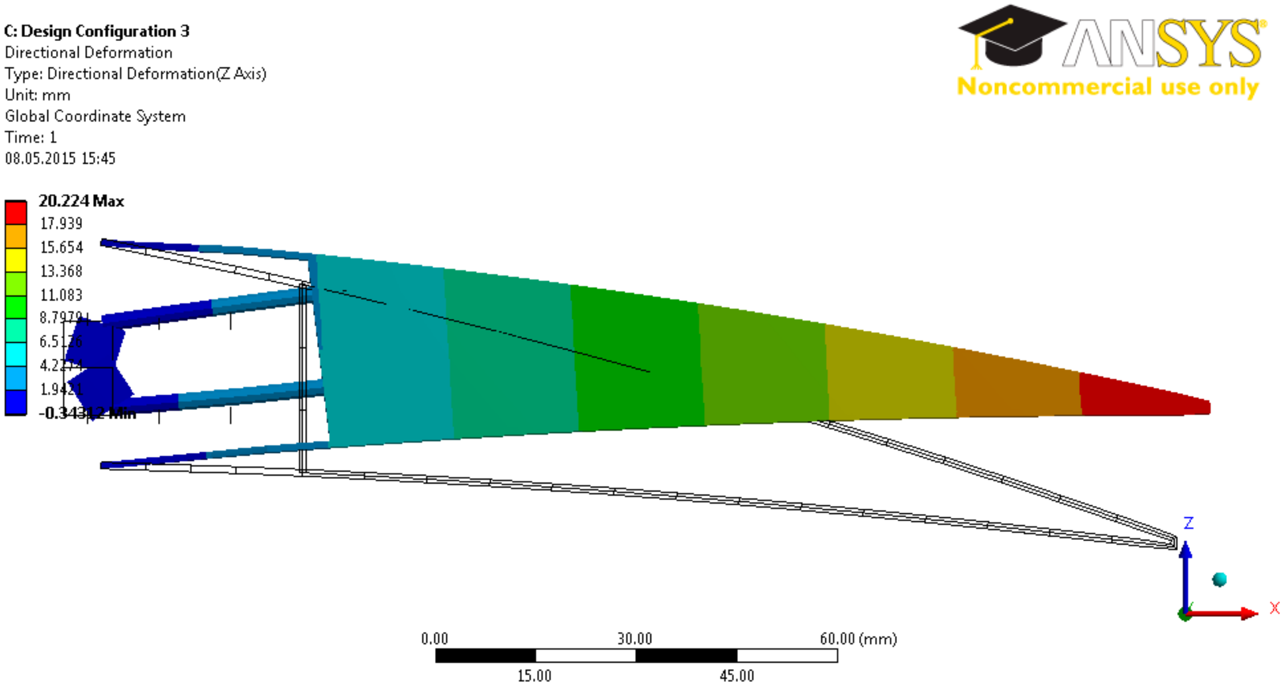

Figure 22. Deformation along *Z*-axis for design configuration 3.

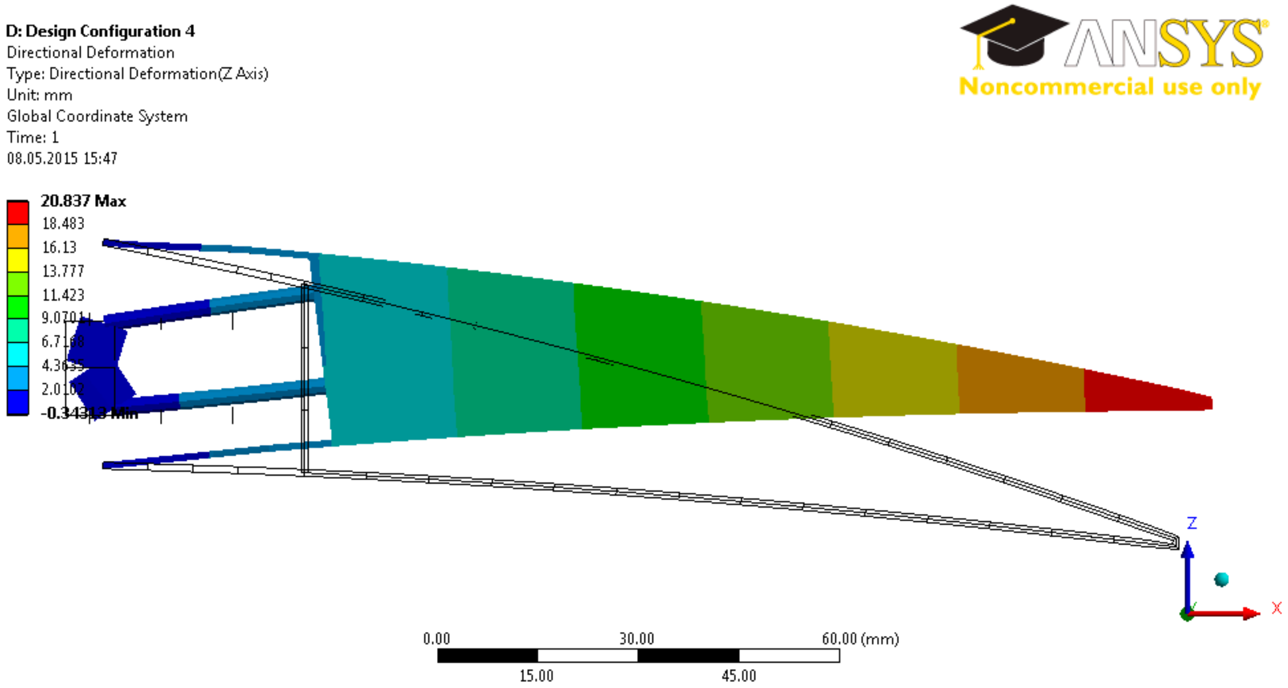

Figure 23. Deformation along *Z*-axis for design configuration 4.

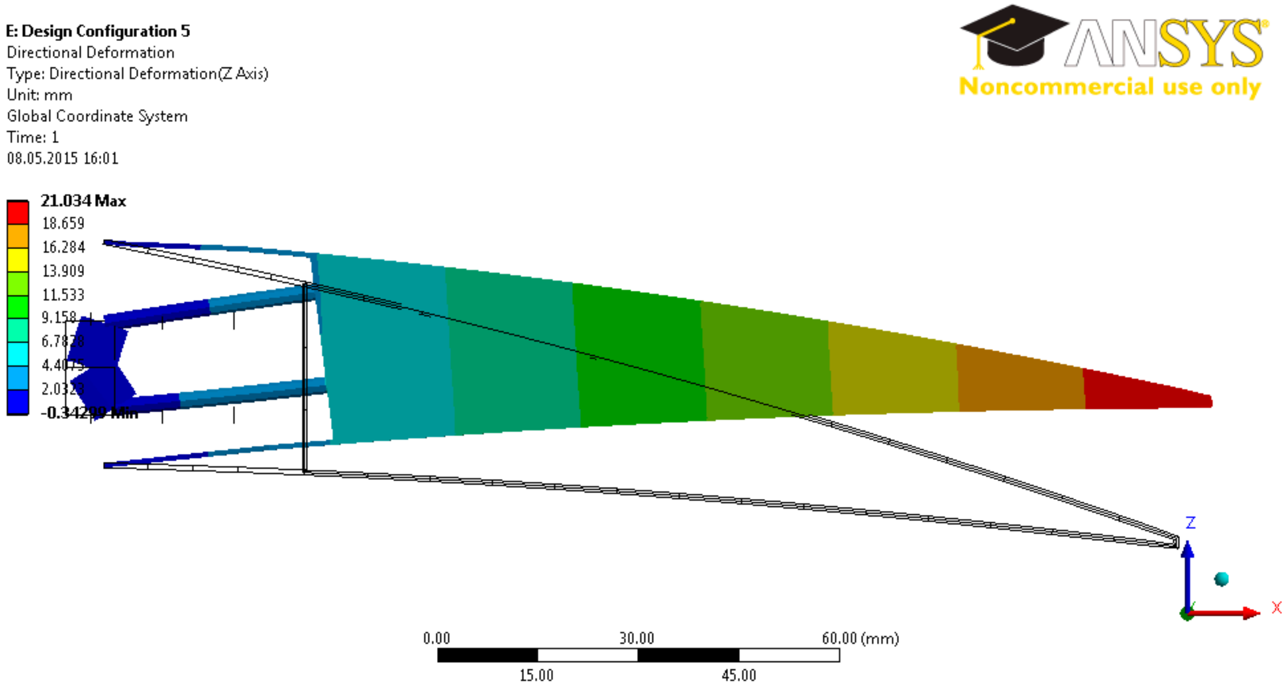

Figure 24. Deformation along *Z*-axis for design configuration 5.

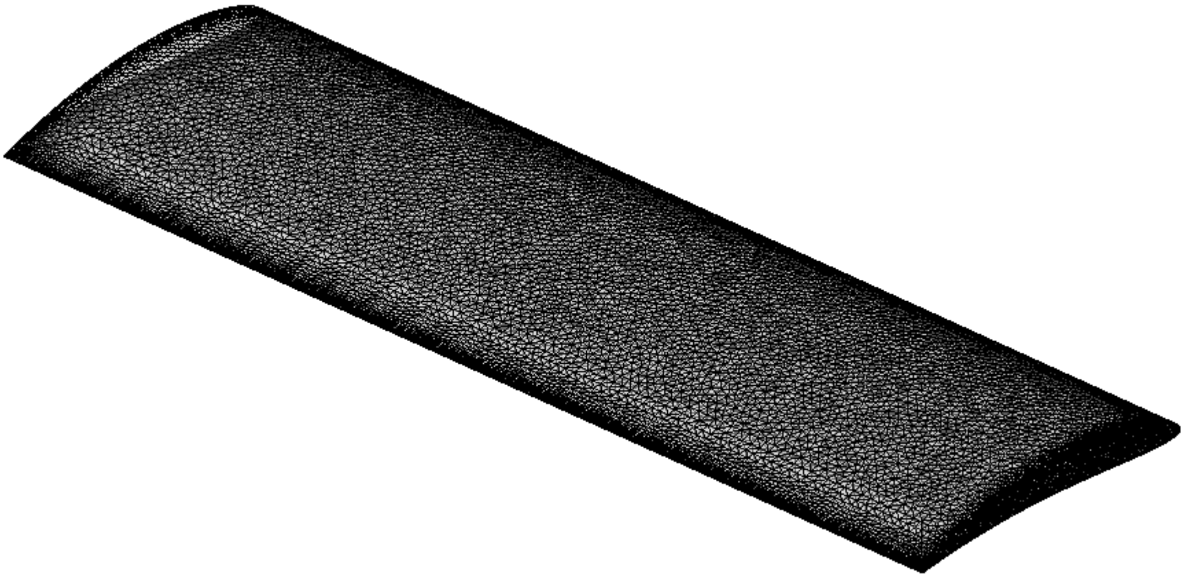

Figure 25. Generated aerodynamic mesh over the wing.

Table 7 provides some additional information about the results for structural analyses, such as the maximum stress values for all the design configurations.

Table 7. Results summary of structural analyses of all design configurations.

Configuration Number	Maximum Combined Bending Stress (Mpa)	Maximum Required Torque (N-mm)	Max Principal Stress on the Composite (MPa)	Max Principal Strain on the Compliant Part
1	63.485	178.950	63.629	0.35131
2	72.188	534.280	214.610	0.22670
3	129.010	1086.800	8.925	0.32670
4	141.980	765.060	6.996	0.32230
5	144.980	582.170	6.886	0.31885

Even though neoprene material gives satisfactory results in design configuration 1, since the material with required properties was only theoretically available, this was considered only a test case and in all other configurations a different compliant material than that of Configuration 1 were used. Configuration 3 utilizes a closed cell design, as compared to Configuration 2, which uses an open cell design. The closed cell design was introduced with the aim of increasing the stiffness of the composite part of the control surface. The results indicated that Configuration 2 was insufficient to provide the required displacements and preserve the shape of the control surface. Furthermore, Configuration 3 resulted in increased torque values. As a result, the number of servo actuators were then increased and the new condition is studied as Configuration 4. Nevertheless, high torque values were encountered and, in order to overcome this problem, the skin thicknesses were reduced in Configuration 5. It was later found that this configuration can maintain the desired profile shape within the torque limits of available servo actuators.

Configuration 5, which is considered as the most optimum design among five configurations considered, was later structurally analyzed under the simulated aerodynamic loading. This was done in order to show that the developed trailing edge also performs well under the aerodynamic loading that the control surface could be subjected to within the operational flight profile of the UAV.

5. Aerodynamic Load Computation

The aerodynamic loading that the trailing edge may be subjected to was computed by considering the intended morphed shape of the control surface and the intended flight profile of the Unmanned Aerial Vehicle to which the developed control surface will be applied.

5.1. CFD Meshing

In order to perform the CFD analysis, one should prepare a mesh which represents the desired geometry and flow field around the geometry. In this analysis, hemisphere domain was used as the far field geometry. This mesh was prepared by using Pointwise® V17.2R2 package program (Pointwise Inc., Fort Worth, TX, USA). The generated mesh has the following properties:

- The average element size was 8 mm. Unstructured triangular was used to model the surface of the wing.
- Some mesh refinement techniques are applied on the leading edge of the wing to capture the presence of high curvature there.
- The radius of the outer hemisphere of the geometry was taken as 20 times the chord length of the wing.
- In order to be able use RANS solver, boundary layer mesh around the wing was modelled by using T-Rex meshing capability of Pointwise.

The mesh over the wing is shown in Figure 25, the boundary layer mesh is illustrated in Figure 26 and the outer domain mesh is depicted in Figure 27.

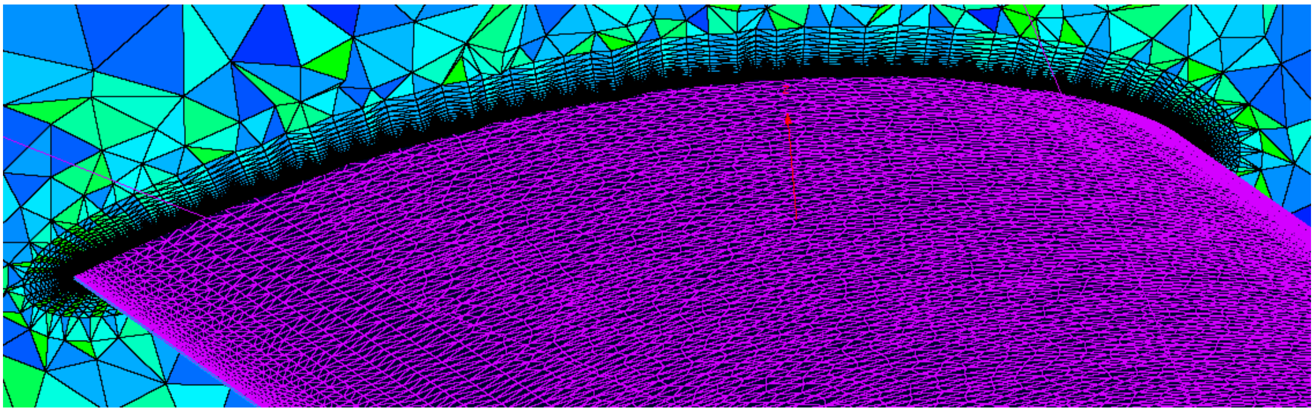

Figure 26. Generated boundary layer mesh over the wing surface.

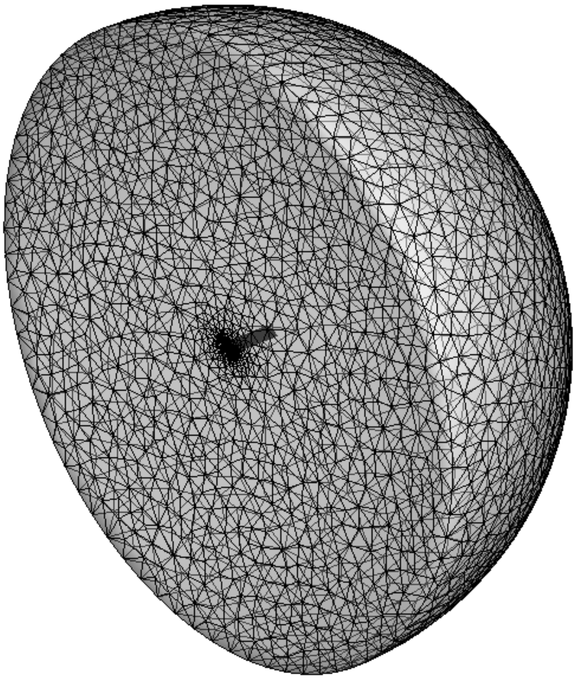

Figure 27. Generated hemisphere outer domain mesh.

5.2. CFD Analysis

Computational fluid dynamics (CFD) analyses were conducted by using Stanford University Unstructured (SU2) V3.2.3 [17] open-source software, which was used as a solver. The SU2 CFD simulation requires both configuration file and the mesh file as its inputs. The former input was prepared according to flight parameters, and the latter input was generated directly by Pointwise® V17.2R2 package program.

The flight parameters defined to the solver are presented in Table 8. These parameters are derived by considering the intended flight profile under 1 g condition of the Unmanned Aerial Vehicle to which the developed trailing edge control surface will be attached to [11]. Incompressible RANS with Spalart–Allmaras turbulence modeling was utilized in the flow solver.

Table 8. Summary of flight parameter used in the CFD analysis.

Parameters	**Landing Phase**	**Take-off Phase**	**Cruise or High Speed Dash Phase**
Flight Speed (m/s)	13.244	21.152	30.556
Angle of Attack (deg)	6.373	1.713	1.056
Reynolds Number	524,536	857,990	1,210,135
Density (kg/m^3)	1.189	1.225	1.189
Mach Number	0.039	0.063	0.090
Altitude (ft)	1000	0	1000

Only a high speed flight condition was examined to check the design capability, since that configuration corresponds to maximum shape changing for the control surface. The contour of pressure coefficient for this configuration was shown in Figure 28.

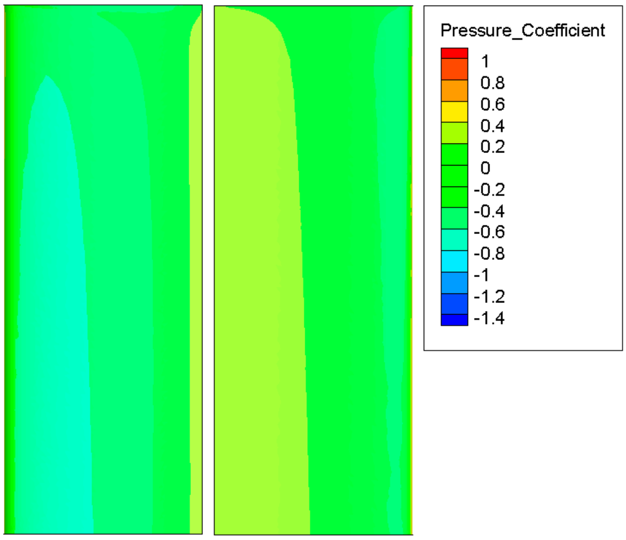

Figure 28. Contour of pressure coefficient corresponding to high speed flow configuration.

This pressure coefficient is then multiplied by dynamic pressure of the flow field to determine the gauge pressure. Later, this gauge pressure was considered as the external load imported for the structural analysis. The displacement results of Configuration 5 under aerodynamic loading are shown in Figure 29.

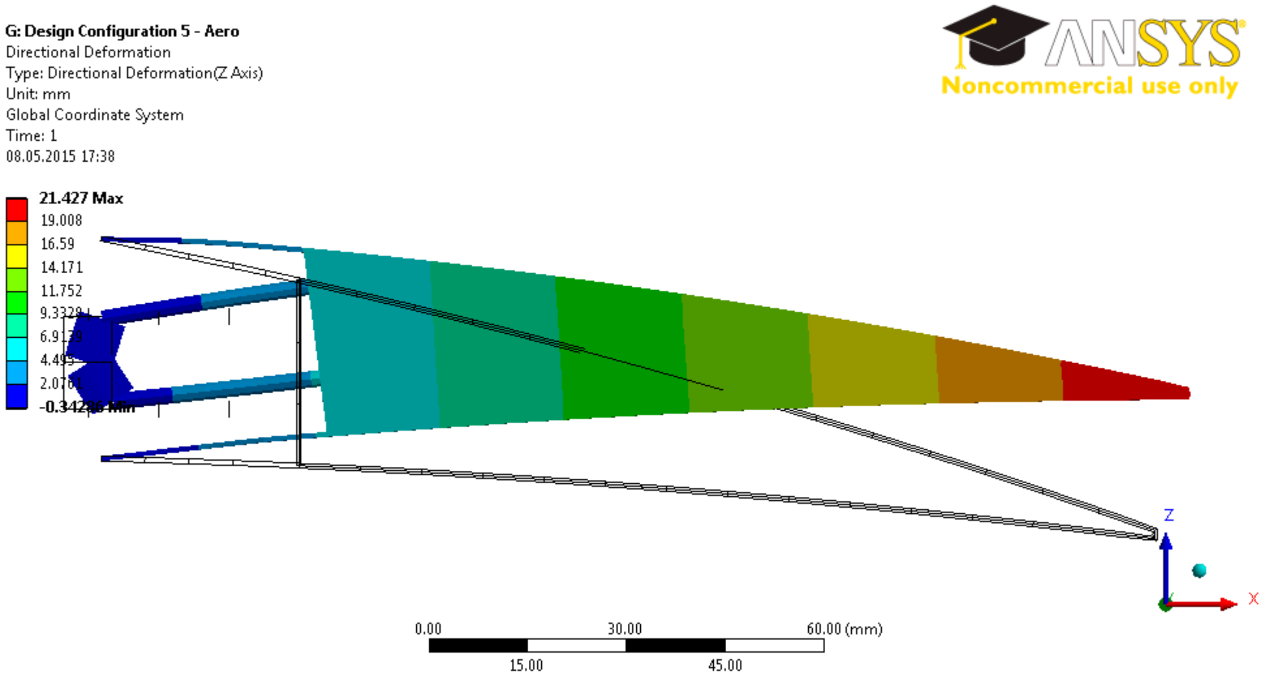

Figure 29. Direction deformation along *Z*-axis for design configuration 5 under aerodynamic loading.

It is found that the maximum required torque for Configuration 5, in order to maintain the desired morphing shape of NACA 2510, was 528.210 N-mm. This value could sufficiently be provided by the total servo actuators. This proved that the best viable design configuration of *in vacuo* analysis also provided the required torque and morphed into the required shape of NACA2510 under the aerodynamic loading as well.

6. Conclusions

This paper describes the design and analyses of a hybrid trailing edge control surface developed for an unmanned aerial vehicle. The hybrid trailing edge was composed of aluminum, composite, and compliant materials. The actuation was provided by miniature servo actuators placed inside the trailing edge. Various configurations which include different number of actuators and/or different geometric shapes were studied *in vacuo* and under aerodynamic loading. Extensive simulations showed that the developed design can perform the required decamber characteristics.

As a future work the wind tunnel tests are also envisaged to further prove the applicability of the developed trailing edge for real flight conditions.

Acknowledgments

The work presented herein has been partially funded by the European Community's Seventh Framework Program (FP7) under the Grant Agreement 314139. The CHANGE project ("Combined morphing assessment software using flight envelope data and mission based morphing prototype wing development") is a L1 project funded under the topic AAT.2012.1.1-2 involving nine partners. The project started in 1 August, 2012.

İlhan Ozan Tunçöz and Yosheph Yang thank TUBITAK (The Scientific and Technological Research Council of Turkey) for supporting them during their graduate education.

Author Contributions

Aerodynamic analyses were conducted by Yosheph Yang and Serkan Özgen. Material studies were undertaken by Pınar Arslan and Ercan Gürses. Uğur Kalkan, Harun Tıraş, İlhan Ozan Tunçöz, Melin Şahin and Yavuz Yaman were involved in structural modelling and analyses.

Conflicts of Interest

The authors declare no conflict of interest.

References

1. Skillen, M.D.; Crossley, W.A. *Modeling and Optimization for Morphing Wing Concept Generation*; NASA/CR-2007-214860; NASA: Hampton, VA, USA, 2007; p. 27.
2. Bolonkin, A.; Gilyard, G.B. *Estimated Benefits of Variable-Geometry Wing Camber Control for Transport Aircraft*; NASA/TM-1999-206586; NASA: Hampton, VA, USA, 1999.
3. Barbarino, S.; Bilgen, O.; Ajaj, R.M.; Friswell, M.I.; Inman, D.J. A review of morphing aircraft. *J. Intell. Mater. Syst. Struct.* **2011**, *22*, 823–877.
4. Friswell, M.I.; Inman, D.J. Morphing concepts for UAVs. In Proceedings of the 21st Bristol UAV System Conference, Bristol, UK, 3–5 April 2006.
5. Shili, L.; Wenjie, G.; Shujun, L. Optimal design of compliant trailing edge for shape changing. *Chin. J. Aeronaut.* **2008**, *21*, 187–192.

6. Bartley-Cho, J.D.; Wang, D.P.; Martin, C.A.; Kudva, J.N.; West, M.N. Development of high-rate, adaptive trailing edge control surface for the smart wing phase 2 wind tunnel model. *J. Intell. Mater. Syst. Struct.* **2004**, *15*, 279–291.
7. Monner, H.P. Realization of an optimized wing camber by using formvariable flap structures. *Aerosp. Sci. Technol.* **2001**, *5*, 445–455.
8. Hilbig, H.; Wagner, H. Variable Wing Camber Control for Civil Transport Aircraft. In Proceedings of 14th Congress of the International Council of the Aeronautical Sciences, Toulouse, France, 10–14 September 1984; ICAS 84-5.2.1.
9. Campanile, L.F.; Sachau, D. The Belt-rib concept: A structronic approach to variable camber. *J. Intell. Mater. Syst. Struct*. **2000**, 11, 215–224.
10. Tunçöz, İ.O. Design and Analysis of a Hybrid Trailing Edge Control Surface of a Fully Morphing Unmanned Aerial Vehicle Wing. Master's Thesis, Middle East Techical University, Ankara, Turkey, February 2015.
11. CHANGE Project. Available online: http://change.tekever.com/ (accessed on 17 May 2015).
12. Rohacell Rima Product Information. Available online: http://www.rohacell.com/sites/dc/Downloadcenter/Evonik/Product/ROHACELL/product-information/ROHACELL%20RIMA%20Product%20Information.pdf (accessed on 17 May 2015).
13. ANSYS Workbench v14.0, Material Library. Available online: http://www.ansys.com (accessed on 17 May 2015).
14. Cambridge University Engineering Department. *Materials Data Book*; Cambridge University: Cambridge, UK, 2003. Available online: http://www-mdp.eng.cam.ac.uk/web/library/enginfo/cueddatabooks/materials.pdf (accessed on 17 May 2015).
15. Invent GmbH. Available online: http://www.invent-gmbh.de/ (accessed on 17 May 2015).
16. Volz Servos. Available online: http://www.volz-servos.com/resources/Downloads/DataSheets/DA_13-05-60_en-m.pdf (accessed on 17 May 2015).
17. Stanford University Unstructured (SU2) V3.2.3. Available online: https://github.com/su2code/SU2/releases/tag/v3.2.3 (accessed on 16 January 2015).